Arteriosclerosis, Thrombosis, and Vascular Biology

TRANSLATIONAL SCIENCES

Analysis of ^{18}F-Sodium Fluoride Positron Emission Tomography Signal Sources in Atherosclerotic Minipigs Shows Specific Binding of ^{18}F-Sodium Fluoride to Plaque Calcifications

Paula Nogales, Carlos Velasco, Adriana Mota-Cobián, Leticia González-Cintado, Rubén Avelino Mota, Samuel España, Jesús Mateo, Jacob F. Bentzon

OBJECTIVE: ^{18}F-sodium fluoride (^{18}F-NaF) positron emission tomography (PET) imaging is thought to visualize active atherosclerotic plaque calcification. This is supported by the binding of ^{18}F-NaF to plaque calcification ex vivo, but no prior studies have examined binding of ^{18}F-NaF to human-like plaque in vivo. Our aim was to validate the specificity of ^{18}F-NaF PET for plaque calcifications in atherosclerotic minipigs.

APPROACH AND RESULTS: Gain-of-function PCSK9^{D374Y} (proprotein convertase/subtilisin kexin type 9) transgenic Yucatan minipigs (n=4) were fed high-fat diet for 2.5 years to develop atherosclerosis and then subjected to ^{18}F-NaF PET/computed tomography imaging. The heart, aorta, and iliac arteries were immediately re-scanned ex vivo after surgical extraction. Lesions from the abdominal aorta, iliac arteries, and coronary arteries were cryo-sectioned for autoradiography. Histological plaque characteristics, PET/computed tomography signal, and autoradiography were linked through regression and co-localization analysis. Arterial ^{18}F-NaF PET signal had intensities comparable to clinical scans and colocalized moderately with calcification detected by computed tomography. Histological analysis showed calcification spanning from microcalcifications near lipid pools and necrotic core to more homogenous macrocalcifications. Comparison with arteries from autopsy cases confirmed the resemblance in localization and appearance with early human plaque calcification. Regression analysis in the abdominal aorta showed correlations with calcified plaque but could not rule out contributions from noncalcified plaque. This was resolved by autoradiography, which showed specific accumulation in plaque calcifications in all examined arteries. In the context of porcine abdominal aorta, ^{18}F-NaF PET imaging was, however, less accurate than computed tomography for detecting small calcifications.

CONCLUSIONS: ^{18}F-NaF accumulates specifically in calcifications of atherosclerotic plaques in vivo.

GRAPHIC ABSTRACT: A graphic abstract is available for this article.

Key Words: atherosclerosis ■ autoradiography ■ computed tomography ■ models, animal ■ positron emission tomography ■ sodium fluoride

See accompanying editorial on page 2585

^{18}F-sodium fluoride (^{18}F-NaF) positron emission tomography/computed tomography (PET/computed tomography [CT]) is a promising noninvasive imaging tool for visualizing active calcification in plaques.[1] Calcifications first appear in progressive lesions near lipid pools and necrotic areas,[2] and ^{18}F-NaF PET may, therefore, provide information about degenerative processes that make plaques dangerous. Although benign lesions in late-stage atherosclerosis are also often calcified, ^{18}F-NaF may bind less to the dense and inert calcifications in such plaques.[3,4] Importantly, increased coronary ^{18}F-NaF uptake was recently shown to predict recurrent events in patients with established coronary atherosclerosis.[5]

See cover image

Correspondence to: Jacob F. Bentzon, MD, PhD, Centro Nacional de Investigaciones Cardiovasculares (CNIC), Calle Melchor Fernández Almagro, 3. CP 28029 Madrid, Spain. Email jfbentzon@cnic.es

The Data Supplement is available with this article at https://www.ahajournals.org/doi/suppl/10.1161/ATVBAHA.121.316075.
For Sources of Funding and Disclosures, see page e489.

Arterioscler Thromb Vasc Biol is available at www.ahajournals.org/journal/atvb

Nonstandard Abbreviations and Acronyms

^{18}F-NaF	^{18}F-sodium fluoride
CT	computed tomography
LAD	left anterior descending
PCSK9	proprotein convertase/subtilisin kexin type 9
PET	positron emission tomography
ROI	region of interest
SUV	standardized uptake value

Highlights

- PCSK9 (proprotein convertase/subtilisin kexin type 9) transgenic minipigs develop plaque calcifications that resemble early human plaque calcifications.
- ^{18}F-sodium fluoride positron emission tomography imaging signal intensity correlates with the amount of plaque calcification in porcine abdominal aorta in vivo and ex vivo.
- Autoradiography shows that ^{18}F-sodium fluoride binds specifically to plaque calcifications, irrespective of their classification as macro- or microcalcifications.
- Similar to human studies, pigs had vascular segments with ^{18}F-sodium fluoride signal despite no computed tomography calcium score. This was explained by reduced specificity and not increased sensitivity of ^{18}F-sodium fluoride positron emission tomography imaging compared with computed tomography.

Whether ^{18}F-NaF localizes specifically to calcifications, or may also bind to other plaque components, has not yet been clarified in vivo for human lesions or experimental lesions with human-like calcification. Previous studies have shown that ^{18}F binds to the surface of calcifications when harvested plaque tissue is incubated with ^{18}F-NaF ex vivo.[3,6,7] Tracer accumulation is, however, not driven exclusively by binding affinity, but also by delivery and washout fluxes,[8] which cannot be modeled ex vivo. For example, blood flow is an important rate-limiting step in bone ^{18}F-NaF imaging.[9]

To study ^{18}F-NaF distribution in plaques in vivo, we used human gain-of-function PCSK9^{D374Y} (proprotein convertase/subtilisin kexin type 9) transgenic minipigs, which feature atherosclerotic plaques that are comparable to human plaques in terms of size and morphology.[10] In the present study, we show that ^{18}F-NaF accumulates specifically in calcifications of plaques in PCSK9^{D374Y} minipigs.

METHODS

The data that support the findings of this study are available from the corresponding author upon request.

Animals

Animal procedures were approved by the Animal Protection Area of the Comunidad Autónoma de Madrid (PROEX265/16) and followed 3R principles to include the minimum number of animals required for sufficient statistical power. Yucatan minipigs (females, n=4) with hepatic overexpression of a human gain-of-function mutant of proprotein convertase/subtilisin kexin type 9 (PCSK9^{D374Y}) were housed in a specific pathogen-free facility. Only females were used to allow nonsurgical urinary catherization during scans. PCSK9^{D374Y} transgenic minipigs were fed standard pig feed supplemented with 20% w/w lard and 2% w/w cholesterol from 2 to 3 until 18 to 22 months of age, and then with feed supplemented with 20% w/w lard alone until termination. Plasma total cholesterol levels were 9.77±2.37 mmol/L at termination.

Human Plaque

Sections of human coronary plaques were obtained from a previously described autopsy material.[11] Material was collected at the Department of Forensic Medicine, University of Aarhus, under ethical permission from the Regional Research Ethics Committee. For subjects <45 years (n=47), artery specimens were not decalcified. From these subjects, we selected sections from the most diseased segment if that was classified as a progressive lesion type (pathological intimal thickening, fibroatheroma, or fibrocalcific plaque) by the classification scheme devised by Virmani et al.[12] A total of 26 left anterior descending (LAD) segments and 24 right coronary artery segments from 30 subjects fulfilled these selection criteria.

In Vivo and Ex Vivo ^{18}F-NaF PET/CT Imaging and Analysis

At 33 months of age (131±8 kg of body weight), pigs underwent clinical ^{18}F-NaF PET/CT scans covering the entire aorta and the iliac arteries. For this purpose, they were fasted overnight and sedated with an intramuscular injection of 20 mg/kg Ketamine, 2 mg/kg Xylazine, and 0.5 mg/kg Midazolam. Following tracheal and urinal intubation, general anesthesia was maintained with an infusion of 2 g/L Ketamine and 0.2 g/L Midazolam with an infusion rate of 2 to 4 mL/kg per hour. ^{18}F-NaF PET/CT images were acquired using a Gemini TF-64 scanner (Philips Healthcare). Animals were imaged in the supine position. Each imaging sequence consisted of low-dose CT (120 kV and 200 mA) followed by PET at 3 hours after the intravenous injection of 654±47 MBq of ^{18}F-NaF. A relatively high dose was used to provide enough activity for subsequent ex vivo scans and autoradiography. The PET/CT scan covered the entire aorta and the iliac arteries. The PET scan was acquired over 10 bed positions with 50% bed overlap (3 minutes per bed) to ensure uniform sensitivity across the region of interest. Finally, coronary computed tomographic angiography with iodinated contrast agent (1.2 mL/kg, Iomeron 400) was performed. Contrast agent was administered at 3 mL/second via an ear vein and flushed with 15 mL of physiological saline followed by a helical ECG gated CT scan. The diastolic phase was selected for the analysis. PET

images were reconstructed using the scanner-implemented LOR-RAMLA algorithm using corrections for normalization, dead time, attenuation, scatter, random events, sensitivity, and decay. The final image matrix contained 234 slices of 144×144 voxels, with 4.0×4.0×4.0 mm^3 voxel size. Low-dose CT images were used for attenuation correction. PET images were fused with the coronary CT angiography image to provide an anatomic reference for the delineation of the coronary arteries or fused with the low-dose CT for the delineation of the abdominal aorta and iliac arteries.

Immediately after the in vivo ^{18}F-NaF PET/CT scan, animals were euthanized by injection of pentobarbital (50 mg/kg), and the heart, the aorta including the iliac bifurcation and the renal arteries were flushed with saline and re-scanned ex vivo using the same settings. In one pig, ex vivo scanning was not possible due to scanner breakdown.

PET and CT images were fused and regions-of-interest (ROIs) were drawn around the arterial profile in CT image slices covering the abdominal aorta from the iliac bifurcation to the right renal artery, the proximal LAD coronary artery and both iliac arteries. Activity concentrations within these ROIs were then quantified in the aligned PET images as standardized uptake values. Maximum and mean standardized uptake value were measured in each ROI, and target-to-background ratios (TBR_{mean} and TBR_{max}) were obtained by dividing SUV_{mean} and SUV_{max} values with the average activity measured in ROIs placed within the abdominal vena cava (for abdominal aorta and iliac arteries) or left ventricle (for coronary arteries). A calcium score was calculated in each CT slice of abdominal aorta by multiplying the number of voxels with attenuation exceeding 130 Hounsfield units or 64 Hounsfield units by the mean attenuation level in those voxels. This value was then divided with the number of voxels in the ROI area to normalize for the difference in vessel profile size along the abdominal aorta. Measurements were performed in MATLAB (Mathworks, Inc).

Histology

Serial sections from the abdominal aorta (every 4 mm from the right renal artery to the iliac bifurcation) were stained with Masson's trichrome to measure the plaque area (or in healthy vessel segments intima area), and by Alizarin Red (A5533, Sigma-Aldrich) to quantify calcified and noncalcified plaque components using the ROI and threshold tools in ImageJ. Human sections were stained with Alizarin Red.

Regression Analysis in the Abdominal Aorta

A segment-based regression analysis between arterial histology and PET signal was conducted in the abdominal aorta. Segments consisted of 3 PET slices (12 mm) or 2 PET slices (8 mm) for the analysis of in vivo and ex vivo scans, respectively. PET signal intensity in each segment was calculated as an average of signal in the 2 to 3 slices (TBRmean/TBRmax and SUVmean/SUVmax for in vivo and ex vivo, respectively). The amount of plaque or intima, calcified plaque, and noncalcified plaque in each segment was estimated from histological sections. Each histological section was first mapped to its location in the in vivo PET/CT scan and linear interpolations were then used to provide estimates of the average cross-sectional areas of the different arterial components within each aortic segment. Holes in sections caused by the breaking of calcified material were interpreted as belonging to the calcified area. Associations between PET measures and the average area of calcified and noncalcified plaque/intima was examined by linear regression.

Autoradiography

Arterial slices of the proximal LAD and right coronary artery, the mid-portion of the thoracic aorta, the distal abdominal aorta and the proximal iliac arteries were rapidly obtained after the ex vivo PET/CT scan, embedded in OCT compound and snap-frozen. Two sections from each block were cut at 40 µm thickness and immediately placed on phosphor imaging plates along with a standard curve consisting of ^{18}F-NaF drops with known activity. After >12 hours, screens were developed on a phosphorimager. Tissue sections were subsequently stained with Alizarin Red for calcification detection. Consecutive thin sections (4 µm) from the same blocks were stained with anti-CD68 antibody (MCA2317GA, BioRad) to detect macrophages. Histological images and autoradiography were aligned and the accumulation of ^{18}F in different plaque components were analyzed by regression and colocalization analysis. For regression analysis each vessel profile was divided into quadrants. In each quadrant, we determined (1) the intensity of the autoradiography signal, adjusted for injected dose, timing and body weight of the pig (standard uptake value) and quantified according to the standard curve of ^{18}F-NaF; (2) percentage of quadrant area covered by calcification in Alizarin Red-stained sections, which was further divided into microcalcification and macrocalcification using an area cutoff of 1963 µm^2 (corresponding to the diameter cut-off of 50 µm—assuming circular shape—that is often used in histological analysis[3]); (3) percentage of quadrant covered by noncalcified tissue calculated as total vessel area—calcified tissue; and (4) percentage of quadrant covered by macrophages. The association of the different histological features and autoradiography signal was analyzed by linear regression. For direct colocalization analysis, ROIs covering calcified areas in the Alizarin Red-stained section were determined with the threshold tool in ImageJ, and the ROIs for calcified tissues were subsequently enlarged by 150 µm to compensate for limitations in autoradiography resolution. Total vessel and lumen areas was outlined manually and total vessel area—(calcified area+lumen area) defined the noncalcified vessel area. ^{18}F-NaF signal was calculated as detailed above in each ROI in the aligned autoradiography image. Measurements were done MATLAB (Mathworks, Inc).

Statistical Analysis

Linear regression analyses were performed after evaluating normal distribution of residuals and homoscedasticity, and correlation coefficients were compared with Fisher r-z transformation. Spearman correlation was used for autoradiography data that did not meet these assumptions. The Kruskal-Wallis test with Dunn post-test were performed for multiple-group comparison. Receiver-operating-characteristic curves were obtained for detection of small calcifications by CT and ^{18}F-NaF PET, and areas under receiver-operating-characteristic curves were compared as described by Hanley and McNeil.[13] Analysis was performed in Prism (GraphPad Software, Inc) and Excel (Microsoft). All tests were 2-tailed and statistical significance was accepted at the level of $P<0.05$.

RESULTS

Minipigs Develop Plaque Calcifications Resembling Early Human Calcifications

PCSK9^{D374Y} minipigs develop atherosclerosis with predilection sites similar to those of human atherosclerosis, mainly affecting the abdominal aorta, iliac arteries, and coronary arteries.[10] We examined lesion types throughout the abdominal aorta and in the proximal atherosclerosis-susceptible part of the iliac arteries and LAD. Lesions were most advanced in the abdominal aorta where fibroatheromas or large pathological intimal thickenings (PITs) were present in all pigs (Figure 1A through 1D). The other vessels had mainly intimal xanthomas and small PITs.

Calcifications were present in the majority of PITs and fibroatheromas (Figure 1E through 1H). Microcalcifications were mainly located in areas with extracellular lipid pools or necrotic core. Macrocalcifications were located in the same regions and were often, but not always, bordered by lipid pools or necrotic core material.

To compare the plaque calcification in PCSK9^{D374Y} minipigs with early human plaque calcifications, we examined sections from atherosclerotic LAD (n=26) and right coronary artery (n=20) from 30 human subjects <45 years of age (21 men, 9 women). Lesion types included 27 PITs, 13 fibroatheromas, 5 fibrocalcific plaques, and 1 ruptured fibroatheroma. Calcifications were found in 26 lesions and their localization and appearance resembled those observed in pigs ranging from sprinkled microcalcifications near lipid pools and necrotic foci in the central part of plaques to more homogenous areas of calcification in the same regions (Figure 1I through 1L). These observations in human plaques are consistent with previous descriptions of human plaque calcification.[2]

^{18}F-NaF PET Signal Associates With Plaque Calcification

Minipigs underwent a clinical ^{18}F-NaF PET imaging protocol followed by several types of analyses to understand the localization of ^{18}F in plaques. ^{18}F-NaF PET signal, obtained 3 hours after radiotracer injection, was observed from all the examined vessels with signal strengths in the range reported for human scans.[14,15] Values (mean±SD) for abdominal aorta were TBR_{max}=2.48±0.68; for iliac arteries TBR_{max}=1.70±0.64; and for LAD TBR_{max}=1.35±0.57.

To determine the source of the signal, we focused on the abdominal aorta, which has large anatomic dimensions compared with PET resolution and thereby allows analysis of multiple independent segments in each pig (Figure 2A through 2D). Moreover, it contained lesions differing in size and developmental stage, yielding statistical strength to our analysis of plaque-signal relationships.

^{18}F-NaF PET signal quantified as TBR_{max} and TBR_{mean} correlated with the presence of CT-detected calcification across the abdominal aorta, but PET signal was also seen in some CT-negative segments with little plaque

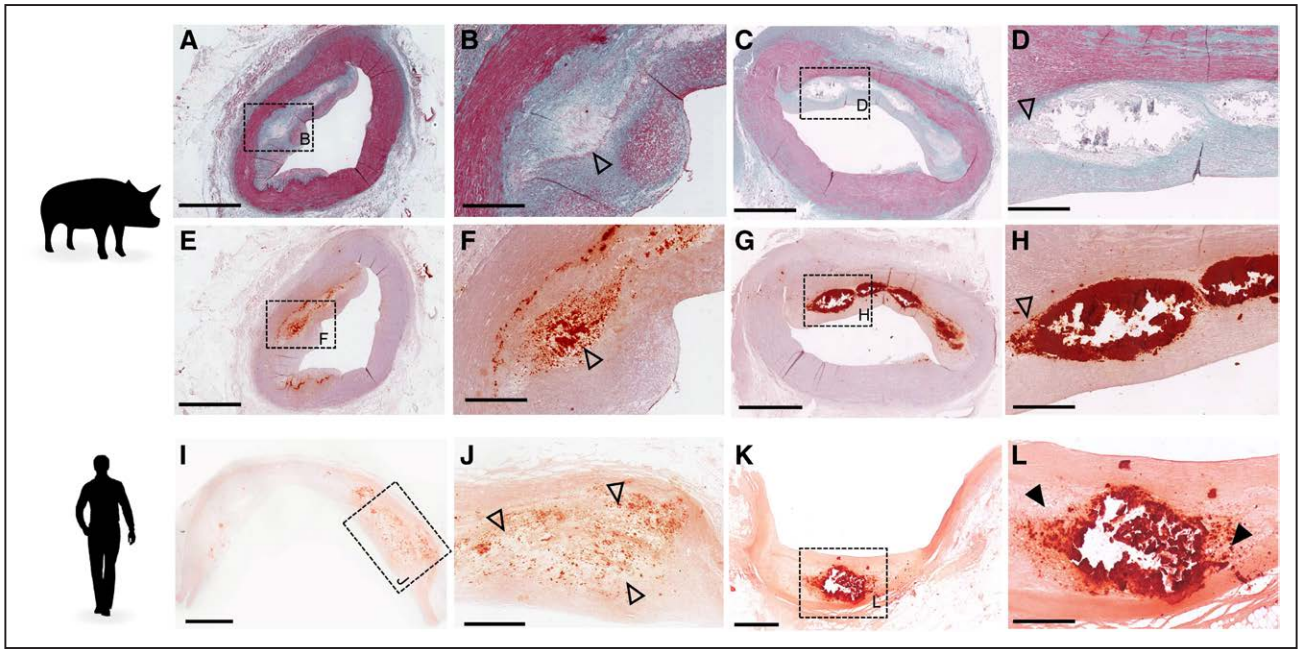

Figure 1. Plaque calcification in PCSK9^{D374Y} (proprotein convertase/subtilisin kexin type 9) minipigs and humans.
A–**D**, Trichrome-stained sections showing lipid pools and early necrotic core formation in abdominal aorta lesions. Insets show selected areas in higher magnification. **E**–**H**, Adjacent sections stained with Alizarin Red. Calcifications range from microcalcifications near lipid pools in the plaque interior to more homogenous calcification in the same region (also leading to some deterioration during sectioning). **I**–**L**, Representative examples of coronary lesions from human subjects (<45 y old) showing a similar range and localization of calcification. Open arrowheads indicate lipid pools and closed arrowheads necrotic core. Scale bars 2.5 mm (**A**, **C**, **E**, and **G**), 1 mm (**I**, **K**), and 0.5 mm (**B**, **D**, **F**, **H**, **J**, **L**).

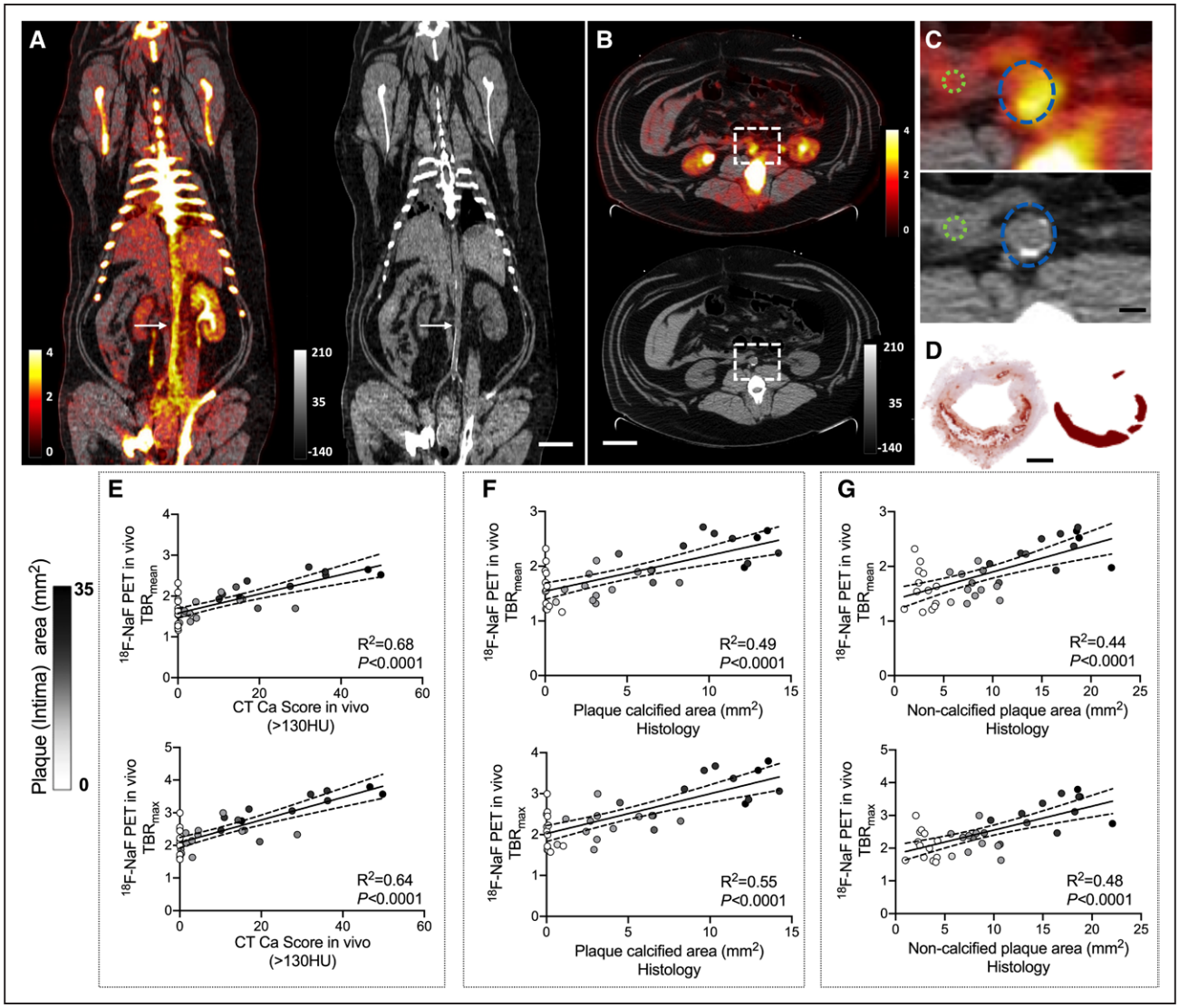

Figure 2. Associations of in vivo ^{18}F-sodium fluoride (^{18}F-NaF) positron emission tomography (PET) signal with computed tomography (CT) and plaque histology.

A–**C**, Fused PET/CT and CT images shown in coronal (**A**) and transversal (**B**), at the level of the arrow) planes. Magnified area with placement of regions of interest for quantification around the aorta (blue) and inside the inferior vena cava (green) are shown in **C**. Scale bars 50 mm (**A** and **B**) and 10 mm (**C**). **D**, Corresponding Alizarin Red-stained section and thresholded signal for calcification showing visual correlations with CT and 18F-NaF signal. Scale bar 2 mm. **E**, Correlations between ^{18}F-NaF PET signal quantified as TBR_{mean} or TBR_{max} and the amount of CT-detected calcification. **F** and **G**, Correlations between ^{18}F-NaF PET signal and the average area of calcified and noncalcified plaque determined by histology. Data points in all panels represent the average value within 12 mm segments of the abdominal aorta. Regression lines with 95% CIs are shown. The color of the data points shows total plaque (intima) area in each segment and indicates the close associations among the size of total, calcified, and noncalcified plaque across segments, which complicates interpretation of the univariate correlations.

formation (Figure 2E). Clear univariate correlations were observed between ^{18}F-NaF PET signal and the amount of plaque calcification determined histologically (Figure 2F). This is consistent with preferential binding of ^{18}F-NaF to plaque calcifications but does not rule out that ^{18}F-NaF could bind other arterial wall components that may evolve in parallel with calcifications. Indeed, we also found significant correlations with noncalcified plaque (Figure 2G). Because of the close relationship between the amount of total plaque, calcified plaque, and noncalcified plaque in our data material, it was not possible with the univariate correlation approach to determine which of these correlations were real and which may be caused by confounding factors.

^{18}F-NaF PET signal in ex vivo scans correlated well with in vivo scan signal across abdominal aortic segments, as expected when the signal originates mainly from the arterial tissue and not background (Figure 3A through 3D). Correlations between ex vivo ^{18}F-NaF PET signal and the size of calcified and noncalcified plaque were similar to the analysis of in vivo scans (Figure 3E and 3F).

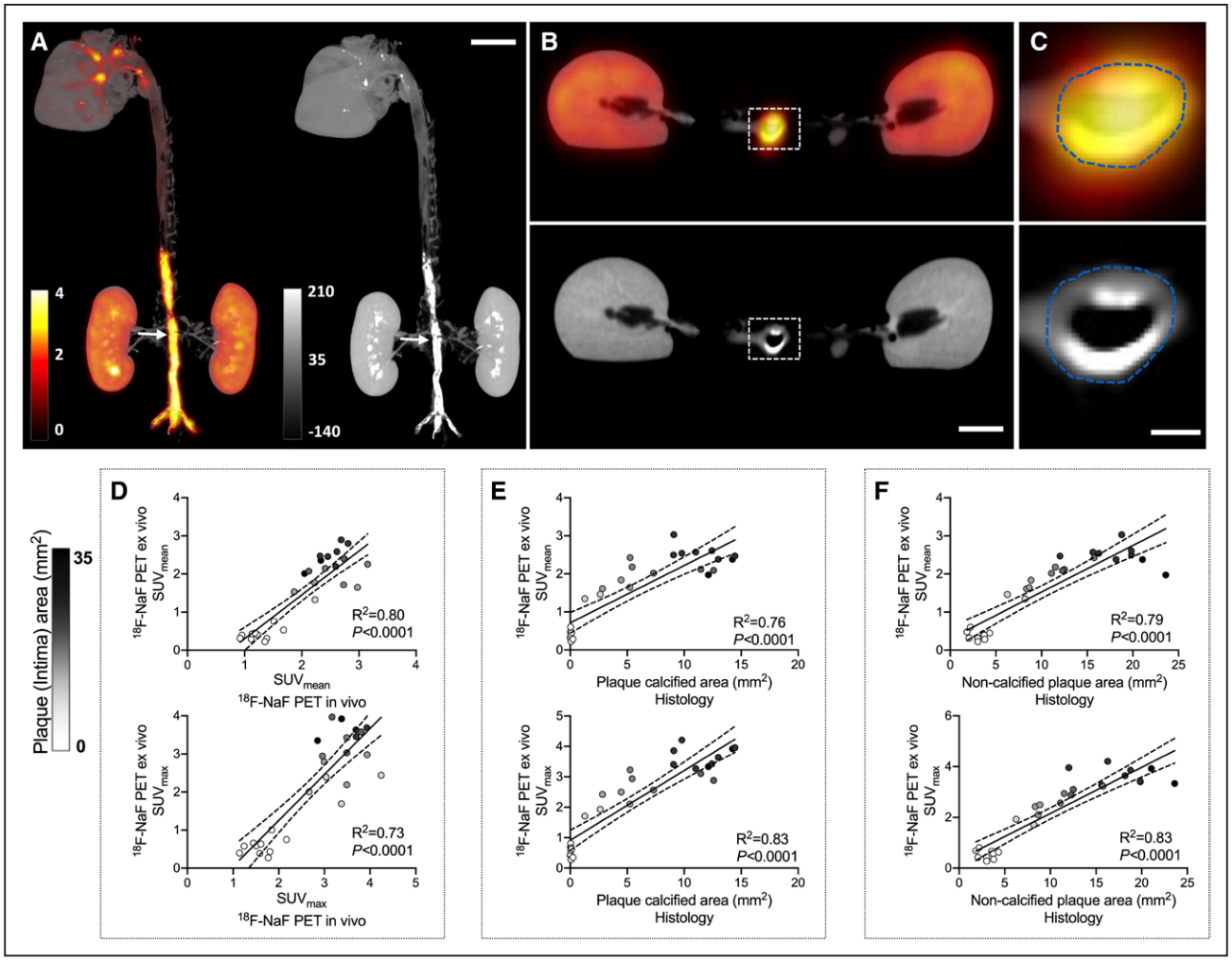

Figure 3. Associations of ex vivo ^{18}F-sodium fluoride (18F-NaF) positron emission tomography signal with plaque histology. **A**–**C**, Fused positron emission tomography (PET)/computed tomography (CT) and CT images shown in coronal (**A**) and transversal (**B**, at the level of the arrow) planes. Magnified area with region of interest around the aorta is shown in **C**. Scale bars 35 mm (**A** and **B**) and 5 mm (**C**). **D**, Correlation between ^{18}F-NaF PET signal obtained ex vivo and in vivo quantified as SUV_{mean} or SUV_{max}. **E** and **F**, Correlations of ^{18}F-NaF PET signal and the amount of calcified (**E**) and noncalcified plaque (**F**) determined by histology. Data points in all panels represent the average value within 8 mm segments of the abdominal aorta. Regression lines with 95% CIs are shown. The color of the data points shows total plaque/intima area in each segment.

Autoradiography Reveals Specific Accumulation of ^{18}F-NaF in Calcified Plaque Regions

To determine the localization of ^{18}F-NaF in plaque, autoradiography analysis was carried out. Signal was recorded from thick cryosections obtained rapidly after ex vivo scans from the abdominal aorta, thoracic aorta, iliac arteries, LAD, and right coronary artery. By visual inspection, the autoradiography signal matched the pattern of subsequent Alizarin Red staining of the sections (Figure 4A and 4B). Sparse signal was seen in the arterial media and in noncalcified plaque regions.

Quantification of plaque-signal relationships was first approached by correlation analysis. This approach has the advantage that it can probe for binding of ^{18}F-NaF to plaque components that are small compared with autoradiography resolution. For this analysis, vessels were divided into quadrants. Because calcifications are not homogenously distributed across the lesion, dividing the vessel profiles into quadrants obviated the correlation between calcified and noncalcified tissue that limited the in vivo analysis (r=0.15, nonsignificant, across quadrants) and allowed us to test for the independent contribution of each tissue type. Significant correlation was found between the areas of ^{18}F-NaF autoradiography signal and calcification (r=0.69, P<0.0001), but not between autoradiography signal and noncalcified tissue (r<0.01, nonsignificant) (Figure 4C and 4D). The association between calcification and autoradiographic signal was observed in both abdominal aorta, iliac artery, and LAD plaques.

Previous studies have proposed that microcalcifications are more effective in binding ^{18}F-NaF than

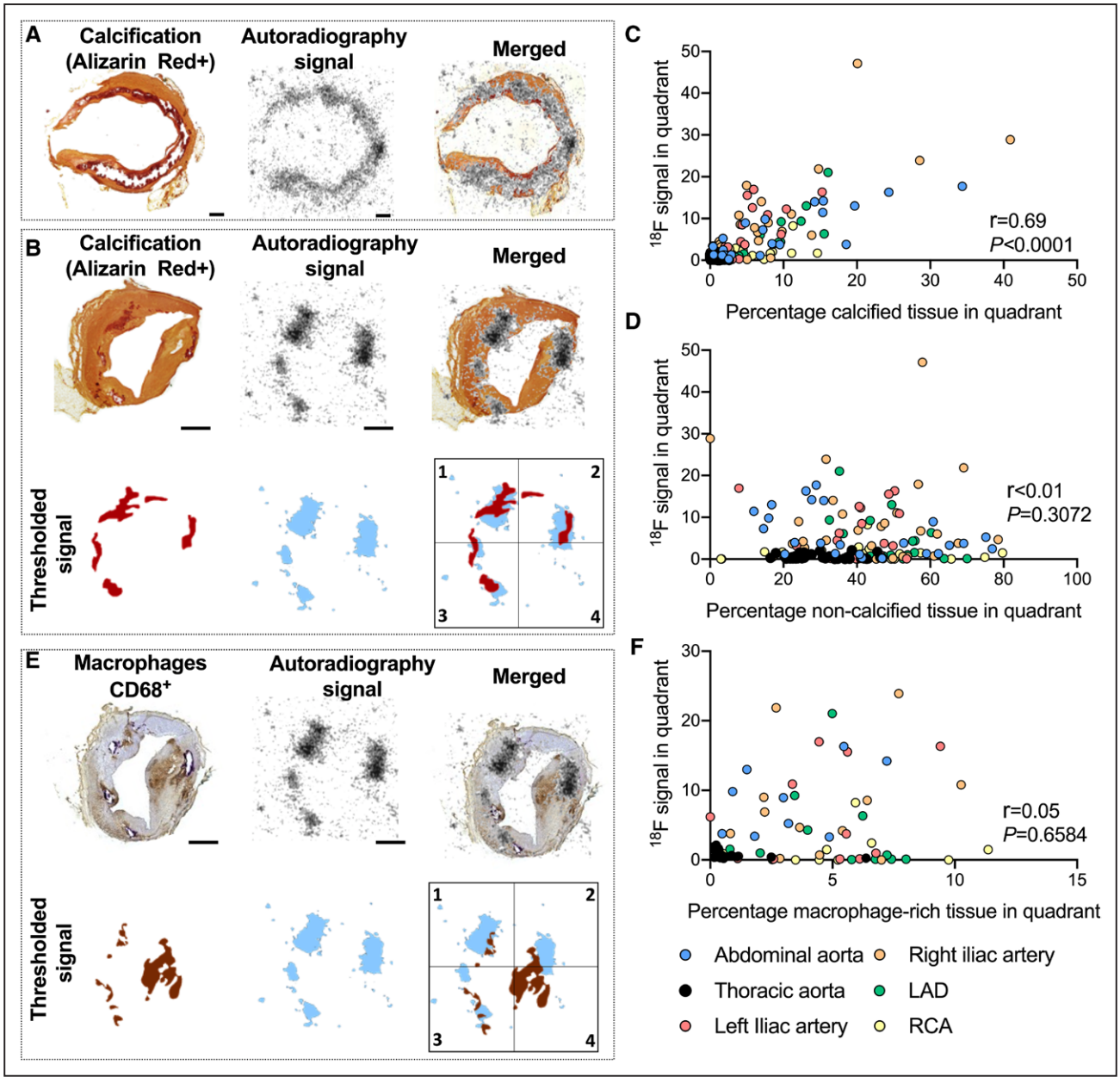

Figure 4. Autoradiography shows specific accumulation of ^{18}F-sodium fluoride (^{18}F-NaF) in plaque calcifications.
A and **B**, Representative examples of Alizarin Red staining, ^{18}F-NaF autoradiography, and the merged image showing visual concordance of ^{18}F-NaF signal and calcification in sections from abdominal aorta (**A**) and left iliac artery (**B**). **C** and **D**, For quantification, the vessel profile was divided into quadrants as indicated in **B**, and the association of total autoradiography signal, normalized among pigs as described in methods, and the percentage covered by calcified (**C**) and noncalcified tissue (**D**) was analyzed by Spearman correlation. Only calcified tissue was significantly associated with ^{18}F signal. **E**, Representative example of macrophage (CD68) staining, ^{18}F-NaF autoradiography, and the merged image from left iliac artery. The thresholded signal illustrates the lack of co-localization of macrophages with ^{18}F autoradiography signal. **F**, Correlation analysis of ^{18}F signal in quadrants with the area fraction covered by macrophages showed no significant association (Spearman correlation). Scale bars 1 mm. Sections were from multiple vascular beds as indicated by the color coding. LAD indicates left anterior descending; and RCA, right coronary artery.

macrocalcifications.[3,4] The quantitative importance of this for total ^{18}F-NaF plaque signal has, however, not been determined. To explore the importance of microcalcification for ^{18}F-NaF accumulation in plaques in the porcine model, we separated calcification into macro- and microcalcified areas based on an area cutoff of 1963 μm^2 (corresponding to the commonly used diameter cutoff of 50 μm; Figure I in the Data Supplement). The correlation between ^{18}F-NaF signal and macro-calcifications (r=0.55, P<0.0001) was similar to the correlation with total calcifications, while the correlation with micro-calcifications was weaker (r=0.33, P<0.0001). This indicates that the majority of the ^{18}F-NaF signal in the examined lesions accumulates in regions with macrocalcification,

which was also apparent by visual inspection of macrocalcification and autoradiography signal.

Finally, to determine if other plaque features are involved in ^{18}F-NaF uptake, we CD68-stained sections for macrophages (Figure 4E). No correlation was present between macrophage area and ^{18}F-NaF autoradiography signal (r=0.05; P=0.66 Figure 4F).

To confirm the binding of ^{18}F-NaF to calcifications in a direct co-localization analysis, we also measured average autoradiography signal intensity within calcified, noncalcified and lumen areas in the aligned histology and autoradiography images. Signal was on average high in calcified compared with noncalcified regions which, in turn, was not significantly different from noise levels measured in the lumen area (Figure 5A and 5B). It should be noted that some calcified regions had low measured signal intensity. This was more often observed in plaques with small calcifications (as indicated by the grayscale in Figure 5B) and could potentially in those cases be explained by uncertainties in alignment and partial volume effects, which causes small sources of signal to be dispersed over a larger area with lower intensity. Furthermore, holes in disintegrated calcifications were included in the calcified region based on the assumption that they were lost during staining after autoradiography, but it is possible that some were lost before.

CT Versus ^{18}F-NaF for Detection of Plaque Calcification

^{18}F-NaF has been proposed as a more sensitive technique than CT for the detection of small plaque calcifications. Such comparisons are highly context-dependent being influenced among other factors by the level of background signal in different territories. To compare the accuracy of ^{18}F-NaF-based versus CT-based quantification of plaque calcification in our specific setting of porcine abdominal aortic plaques, we conducted association analysis of CT calcium scores using the standard threshold attenuation level of 130 Hounsfield units and a reduced level of 64 Hounsfield units to define calcification. Compared with the similar association analysis for ^{18}F-NaF PET shown in Figure 2F, significantly higher correlation coefficients were obtained (Figure 6A and 6B).[13] The improved correlations were partly explained by better distinction of segments with small calcifications from noncalcified segments, and consistently, CT showed superior sensitivity and specificity for detecting small plaque calcifications in porcine abdominal aorta sections in receiver-operating-characteristic analysis (Figure 6C).

DISCUSSION

Gene-modified minipigs with atherosclerosis offer possibilities to determine the sources of PET signals in a setting that features human-sized arteries and plaques. This adds complementary information to clinical studies where it is generally not possible to determine the localization of in vivo delivered PET tracers within atherosclerotic lesions.

Previous efforts to validate ^{18}F-NaF PET imaging have found that pre-surgical ^{18}F-NaF PET signal in patients undergoing carotid endarterectomy correlates with the amount of calcium deposits in harvested plaque material.[16] Furthermore, it has been shown that ^{18}F-NaF binds the surface of calcifications in ex vivo incubated plaque.[3,17] While these approaches have the clear strength that they can be conducted with human plaques, they also have limitations. First, univariate association analysis cannot predict the physical localization of tracers. In our data set, we saw significant univariate correlations between ^{18}F-NaF PET signal and the amount of noncalcified plaque although ^{18}F-NaF was subsequently found by autoradiography to only accumulate in the calcified region. This is a clear example of how internal correlations between the size of different plaque components, in this case

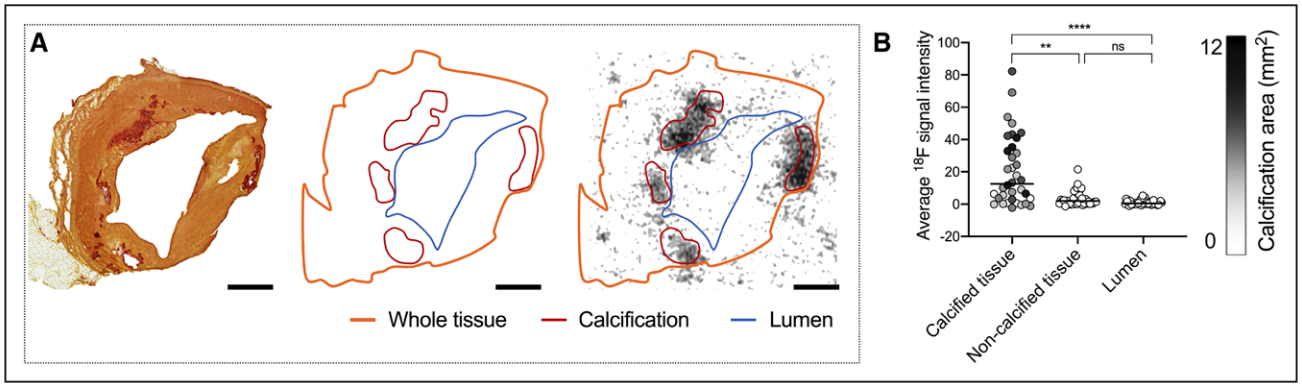

Figure 5. Colocalization analysis of calcified tissue and autoradiography signal.
A, Representative example of Alizarin Red staining with regions of interest (ROIs) for total tissue (orange), calcified tissue (red), and lumen (blue). Total vessel area—(calcified area+lumen area) defined the noncalcified vessel area. **B**, Average ^{18}F signal intensity was high in calcified tissue ROIs, while signal in noncalcified regions was not significantly different from signal (noise) in the lumen area. Kruskal-Wallis test (P<0.0001) with Dunn post-test (****P<0.0001, **P<0.01), The gray scale of the data points in the calcified tissue column shows the calcified ROI size. ns indicates nonsignificant.

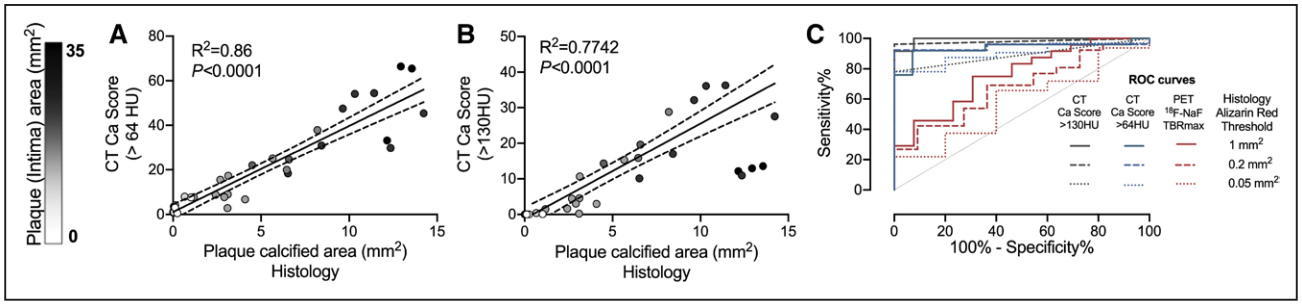

Figure 6. Computed tomography (CT) is superior to ^{18}F-sodium fluoride (^{18}F-NaF) positron emission tomography (PET) for detecting small calcifications in the porcine abdominal aorta.

A and **B**, Correlations between CT calcium scores using the standard threshold attenuation level of 130 HU (**A**) and a reduced level of 64 HU (**B**) to define calcification. Regression lines with 95% CIs are shown. Correlation coefficients were significantly higher than for the similar analysis using TBR_{mean} or TBR_{max} in Figure 2F ($P<0.05$, Fisher r-z transformation, except for CT Ca score HU>130 vs TBR_{max}, which was $P=0.08$). The grayscale of the data points shows total plaque/intima area in each segment. **C**, Receiver-operating characteristic (ROC) curves showing the accuracy of the different modalities in correctly classify vessel segments as calcified/noncalcified at the indicated thresholds for calcification. The area under the ROC curves for the 2 CT scores were significantly higher than for TBR_{max} at each threshold level (all $P<0.05$ by the technique of Hanley and McNeil). Analysis with TBR_{mean} gave similar results (not shown).

between noncalcified and calcified plaque, can drive misleading associations between PET signal and plaque features. Second, ex vivo incubations of plaque tissue do not necessarily mimic the in vivo distribution of tracers, which is determined not only by binding affinity, but also by influx and outflux rates between blood and plaques.[8]

Approaches to Determine Signal Sources in Experimental Models

^{18}F-NaF PET imaging has previously been applied in animal models where plaque calcification occurs, including rabbits and pigs,[18,19] but these prior studies did not study the localization of ^{18}F-NaF in plaques or validated the ability of ^{18}F-NaF PET to measure plaque calcification. In the present study, we carried out analysis for ^{18}F-NaF in plaques in 2 steps. By regression analysis, we found clear associations between the amount of plaque calcification and in vivo and ex vivo PET signal. Yet, this approach could not rule out that ^{18}F-NaF also accumulated in noncalcified plaque because of the high degree of concordance between calcified and noncalcified plaque components across vascular segments in our model. Only by analyzing at the autoradiography level it was possible to demonstrate the specific uptake of ^{18}F-NaF in calcified regions. The amount of calcifications alone correlated with autoradiographic ^{18}F-NaF signal, and co-localization analysis showed autoradiography ^{18}F-NaF signal levels significantly above background levels only in the calcified region.

Macro- Versus Microcalcification

Clinical imaging in patients with symptomatic atherosclerosis has found that arterial segments with CT-detectable calcification in some cases do not have clear ^{18}F-NaF PET signal and vice versa.[1] Evidence from ex vivo incubations of human endarterectomy specimens suggest that this may be because dense macrocalcifications only bind ^{18}F-NaF at the surface, while giving strong CT attenuation. In contrast, microcalcifications can bind more ^{18}F-NaF per volume because of their higher surface-to-volume ratios, but may be too small to increase voxel attenuation to be detected by standard CT calcium scoring.[3]

In our experiments, we found at least moderate levels of ^{18}F-NaF signal in all segments with CT-detectable calcifications. Consistently, macrocalcifications, defined by the commonly used threshold for histology, efficiently bound ^{18}F proportionally to their size in autoradiographic analysis, while microcalcifications were less important for total ^{18}F-NaF signal in accordance with their small contribution to total calcification volume. The efficient ^{18}F-NaF binding to macrocalcifications may reflect the fact that plaques in the porcine model had early types of calcifications, similar to those observed in the human plaque material from persons <45 years. It is conceivable that ^{18}F-NaF can more easily access and bind throughout such loosely organized calcifications compared with the larger and denser calcifications that develop in human plaques with age, often completely precluding cutting in paraffin without decalcification. Furthermore, the calcifications in the pig model are likely developing in size whereas many calcifications in late human plaques may be inert. ^{18}F has been suggested to bind particularly well to sites of active calcification.[9] Unfortunately, there are no current experimental atherosclerosis models that develop densely calcified plaques or allow control of the rate of calcification in which the importance of calcification density or activity could be addressed in vivo.

Similar to clinical studies, we observed some segments that had ^{18}F-NaF signal despite no CT-detectable calcification (Figure 2E). The ability to validate this against histologically verified calcification revealed, however, that the phenomenon did not arise from increased sensitivity of ^{18}F-NaF to detect small calcifications compared with CT, but rather from decreased specificity of the PET signal.

This is not unexpected and caution has previously been raised against overinterpreting the biological meaning of ^{18}F-NaF positive, CT-negative vessel segments.[20] PET has low resolution compared with CT and hence cannot place the origin of imaging signal as precisely as CT. It is therefore expected that some signal from calcifications disperse to slices where CT signal is not seen. It is important to stress that these ^{18}F-NaF PET and CT comparisons are highly context dependent, and it is well possible that the specificity of human coronary ^{18}F-NaF PET imaging is higher than in our experiments where spill-over from the vertebral column and a high dose of ^{18}F-NaF may contribute to higher background signal. CT, on the other hand, performed extremely well in measuring the amount of calcification in the porcine abdominal aorta, and could detect plaques with only 0.05 mm^2 cross-sectional calcified area with good sensitivity and specificity.

Clinical Perspectives

The ^{18}F-NaF PET activity of culprit plaques and the demonstration that high coronary ^{18}F-NaF PET levels are associated with recurrent clinical events suggest that active calcification marks dangerous lesion development.[4,5] Since the development of calcification itself is probably innocent, this is likely because calcification is a telltale of other important disease mechanisms in the plaque. Calcification is typically absent from early human lesions but develop in the interior of pathological intima thickenings and fibroatheromas, where they are often found in areas with lipid pools and in the border zone to necrosis.[21] The precipitation of calcification at these sites seem to be regulated, at least in part, by modulation of SMCs to osteochondrogenic subtypes, which secrete bone-like matrix and regulatory factors as well as calcifying extracellular vesicles that can nucleate hydroxyapatite deposition.[22] How these processes are regulated in plaques will be important to fully understand the information provided by ^{18}F-NaF PET imaging. Using the combination of clinical imaging and the possibility to intervene against disease processes in the PCSK9^{D374Y} minipig may be useful to explore these mechanistic links.

In advanced disease, it cannot be excluded that ^{18}F-NaF can bind thrombotic material or small calcifications that form in organized thrombi.[23,24] Thrombotic complications do not occur spontaneously in experimental models of atherosclerosis, including in PCSK9 transgenic pigs, but the role of thrombosis for ^{18}F-NaF binding could potentially be explored after artificially induced plaque thrombosis or in other experimental models of induced thrombus formation.

Limitations

The present study was based on a small number of pigs, which were all females to allow nonsurgical urinary catherization during scans. These limitations are unlikely to influence on our conclusion that ^{18}F-NaF binds selectively to plaque calcifications, but the small number of pigs meant that some relevant analyses could not be performed including detailed analysis of coronary ^{18}F-NaF -PET imaging. Because of the low resolution of PET and the limited spread of the coronary lesions in the present set of pigs, each pig could only contribute with one data point per coronary artery, which was not enough to perform meaningful regression analysis with the current group size. The autoradiography, however, also included coronary lesions, and, therefore, our description of the physical localization of ^{18}F to sites of calcification also applies to coronary atherosclerosis.

CONCLUSIONS

^{18}F-NaF delivered in vivo accumulates specifically at sites of calcification in PITs and fibroatheromas of minipigs with human-like early plaque calcification.

ARTICLE INFORMATION

Received February 5, 2021; accepted July 8, 2021.

Affiliations

Centro Nacional de Investigaciones Cardiovasculares (CNIC), Madrid, Spain (P.N., C.V., A.M.-C., L.G.-C., R.A.M., S.E., J.M., J.F.B.). Departamento de Estructura de la Materia, Física Térmica y Electrónica, Universidad Complutense de Madrid, IdISSC, Spain (A.M.-C., S.E.). Charles River Laboratories Spain, Sant-Cugat del Vallés (R.A.M.). Heart Diseases and Steno Diabetes Center Aarhus, Department of Clinical Medicine, Aarhus University, Denmark (J.F.B.).

Acknowledgments

We thank the Animal Facility Unit and Histopathology Unit at CNIC for excellent technical help, and the Microscopy Unit at CNIC for expert assistance with automated image analysis.

Sources of Funding

The study was funded by grants from the Ministerio de Ciencia e Innovación (SAF2016-75580-R to J.F. Bentzon and BES-2016-076633 to P. Nogales) and the Instituto de Salud Carlos III (ERA-CVD project SCAN, AC17/00062 to J.F. Bentzon and FIS-FEDER PI14-01427 to J. Mateo) with cofunding from the Fondo Europeo de Desarrollo Regional (FEDER, "Una manera de hacer Europa"). The CNIC is supported by the Instituto de Salud Carlos III, the Ministerio de Ciencia e Innovación and the Pro CNIC Foundation.

Disclosures

None.

Supplemental Materials

Data Supplement Figure I

REFERENCES

1. Tzolos E, Dweck MR. 18F-sodium fluoride (18F-NaF) for imaging microcalcification activity in the cardiovascular system. *Arterioscler Thromb Vasc Biol.* 2020;40:1620–1626. doi: 10.1161/ATVBAHA.120.313785
2. Otsuka F, Sakakura K, Yahagi K, Joner M, Virmani R. Has our understanding of calcification in human coronary atherosclerosis progressed? *Arterioscler Thromb Vasc Biol.* 2014;34:724–736. doi: 10.1161/ATVBAHA.113.302642
3. Irkle A, Vesey AT, Lewis DY, Skepper JN, Bird JL, Dweck MR, Joshi FR, Gallagher FA, Warburton EA, Bennett MR, et al. Identifying active vascular microcalcification by (18)F-sodium fluoride positron emission tomography. *Nat Commun.* 2015;6:7495. doi: 10.1038/ncomms8495

4. Joshi NV, Vesey AT, Williams MC, Shah AS, Calvert PA, Craighead FH, Yeoh SE, Wallace W, Salter D, Fletcher AM, et al. 18F-fluoride positron emission tomography for identification of ruptured and high-risk coronary atherosclerotic plaques: a prospective clinical trial. *Lancet*. 2014;383:705–713. doi: 10.1016/S0140-6736(13)61754-7
5. Kwiecinski J, Tzolos E, Adamson PD, Cadet S, Moss AJ, Joshi N, Williams MC, van Beek EJR, Dey D, Berman DS, et al. Coronary 18F-sodium fluoride uptake predicts outcomes in patients with coronary artery disease. *J Am Coll Cardiol*. 2020;75:3061–3074. doi: 10.1016/j.jacc.2020.04.046
6. Creager MD, Hohl T, Hutcheson JD, Moss AJ, Schlotter F, Blaser MC, Park MA, Lee LH, Singh SA, Alcaide-Corral CJ, et al. 18F-Fluoride signal amplification identifies microcalcifications associated with atherosclerotic plaque instability in positron emission tomography/computed tomography images. *Circ Cardiovasc Imaging*. 2019;12:e007835. doi: 10.1161/CIRCIMAGING.118.007835
7. Youn T, Al'Aref SJ, Narula N, Salvatore S, Pisapia D, Dweck MR, Narula J, Lin FY, Lu Y, Kumar A, et al. 18F-sodium fluoride positron emission tomography/computed tomography in ex vivo human coronary arteries with histological correlation. *Arterioscler Thromb Vasc Biol*. 2020;40:404–411. doi: 10.1161/ATVBAHA.119.312737
8. Libby P, Bhatt DL, Di Carli M. Fluorodeoxyglucose uptake in atheroma: not so simple. *J Am Coll Cardiol*. 2019;74:1233–1236. doi: 10.1016/j.jacc.2019.07.009
9. Czernin J, Satyamurthy N, Schiepers C. Molecular mechanisms of bone 18F-NaF deposition. *J Nucl Med*. 2010;51:1826–1829. doi: 10.2967/jnumed.110.077933
10. Al-Mashhadi RH, Sørensen CB, Kragh PM, Christoffersen C, Mortensen MB, Tolbod LP, Thim T, Du Y, Li J, Liu Y, et al. Familial hypercholesterolemia and atherosclerosis in cloned minipigs created by DNA transposition of a human PCSK9 gain-of-function mutant. *Sci Transl Med*. 2013;5:166ra1. doi: 10.1126/scitranslmed.3004853
11. Dalager S, Paaske WP, Kristensen IB, Laurberg JM, Falk E. Artery-related differences in atherosclerosis expression: implications for atherogenesis and dynamics in intima-media thickness. *Stroke*. 2007;38:2698–2705. doi: 10.1161/STROKEAHA.107.486480
12. Virmani R, Kolodgie FD, Burke AP, Farb A, Schwartz SM. Lessons from sudden coronary death: a comprehensive morphological classification scheme for atherosclerotic lesions. *Arterioscler Thromb Vasc Biol*. 2000;20:1262–1275. doi: 10.1161/01.atv.20.5.1262
13. Hanley JA, McNeil BJ. A method of comparing the areas under receiver operating characteristic curves derived from the same cases. *Radiology*. 1983;148:839–843. doi: 10.1148/radiology.148.3.6878708
14. Dweck MR, Chow MW, Joshi NV, Williams MC, Jones C, Fletcher AM, Richardson H, White A, McKillop G, van Beek EJ, et al. Coronary arterial 18F-sodium fluoride uptake: a novel marker of plaque biology. *J Am Coll Cardiol*. 2012;59:1539–1548. doi: 10.1016/j.jacc.2011.12.037
15. Derlin T, Tóth Z, Papp L, Wisotzki C, Apostolova I, Habermann CR, Mester J, Klutmann S. Correlation of inflammation assessed by 18F-FDG PET, active mineral deposition assessed by 18F-fluoride PET, and vascular calcification in atherosclerotic plaque: a dual-tracer PET/CT study. *J Nucl Med*. 2011;52:1020–1027. doi: 10.2967/jnumed.111.087452
16. Cocker MS, Spence JD, Hammond R, Wells G, deKemp RA, Lum C, Adeeko A, Yaffe MJ, Leung E, Hill A, et al; Canadian Atherosclerosis Imaging Network (CAIN). [18F]-NaF PET/CT identifies active calcification in carotid plaque. *JACC Cardiovasc Imaging*. 2017;10:486–488. doi: 10.1016/j.jcmg.2016.03.005
17. Rudd JH, Warburton EA, Fryer TD, Jones HA, Clark JC, Antoun N, Johnström P, Davenport AP, Kirkpatrick PJ, Arch BN, et al. Imaging atherosclerotic plaque inflammation with [18F]-fluorodeoxyglucose positron emission tomography. *Circulation*. 2002;105:2708–2711. doi: 10.1161/01.cir.0000020548.60110.76
18. Senders ML, Hernot S, Carlucci G, van de Voort JC, Fay F, Calcagno C, Tang J, Alaarg A, Zhao Y, Ishino S, et al. Nanobody-facilitated multiparametric PET/MRI phenotyping of atherosclerosis. *JACC Cardiovasc Imaging*. 2019;12:2015–2026. doi: 10.1016/j.jcmg.2018.07.027
19. McKenney-Drake ML, Moghbel MC, Paydary K, Alloosh M, Houshmand S, Moe S, Salavati A, Sturek JM, Territo PR, Weaver C, et al. 18F-NaF and 18F-FDG as molecular probes in the evaluation of atherosclerosis. *Eur J Nucl Med Mol Imaging*. 2018;45:2190–2200. doi: 10.1007/s00259-018-4078-0
20. Demer LL, Tintut Y, Nguyen KL, Hsiai T, Lee JT. Rigor and reproducibility in analysis of vascular calcification. *Circ Res*. 2017;120:1240–1242. doi: 10.1161/CIRCRESAHA.116.310326
21. Stary HC. The development of calcium deposits in atherosclerotic lesions and their persistence after lipid regression. *Am J Cardiol*. 2001;88:16E–19E. doi: 10.1016/s0002-9149(01)01713-1
22. Nakahara T, Dweck MR, Narula N, Pisapia D, Narula J, Strauss HW. Coronary artery calcification: from mechanism to molecular imaging. *J Am Coll Cardiol Img*. 2017;10:582–593. doi: 10.1016/j.jcmg.2017.03.005
23. Fletcher AJ, Dweck MR. Detecting native and bioprosthetic aortic valve disease using 18F-sodium fluoride: clinical implications. *J Nucl Cardiol*. 2021;28:481–491. doi: 10.1007/s12350-020-02411-x
24. Verma P, Purandare N, Agrawal A, Shah S, Rangarajan V. Unusual finding of a tumor thrombus arising from osteosarcoma detected on 18F-NaF PET/CT. *Clin Nucl Med*. 2016;41:e304–e306. doi: 10.1097/RLU.0000000000001174